Special Collection

Design, Synthesis, *in vitro* and *in silico* Characterization of 2-Quinolone-L-alaninate-1,2,3-triazoles as Antimicrobial Agents

Oussama Moussaoui,*[a] Rajendra Bhadane,[b, c] Riham Sghyar,[a] Janez Ilaš,[d] El Mestafa El Hadrami,[a] Said Chakroune,[a] and Outi M. H. Salo-Ahen*[b, c]

Due to the ever-increasing antimicrobial resistance there is an urgent need to continuously design and develop novel antimicrobial agents. Inspired by the broad antibacterial activities of various heterocyclic compounds such as 2-quinolone derivatives, we designed and synthesized new methyl-(2-oxo-1,2-dihydroquinolin-4-yl)-L-alaninate-1,2,3-triazole derivatives via 1,3-dipolar cycloaddition reaction of 1-propargyl-2-quinolone-L-alaninate with appropriate azide groups. The synthesized compounds were obtained in good yield ranging from 75 to 80%. The chemical structures of these novel hybrid molecules were determined by spectroscopic methods and the antimicrobial activity of the compounds was investigated against both bacterial and fungal strains. The tested compounds showed significant antimicrobial activity and weak to moderate antifungal activity. Despite the evident similarity of the quinolone moiety of our compounds with fluoroquinolones, our compounds do not function by inhibiting DNA gyrase. Computational characterization of the compounds shows that they have attractive physicochemical and pharmacokinetic properties and could serve as templates for developing potential antimicrobial agents for clinical use.

Introduction

In the face of the continuous increase of antimicrobial resistance (AMR), we are on the verge of losing a whole arsenal of antimicrobial compounds that are still effective in the clinic.[1] For example, quinolone antibiotics represent one of the compound classes whose use has been compromised by the increasing emergence of resistant strains.[2] Currently many research groups are working on the design of new antimicrobial drugs and, namely, design of molecules containing heterocyclic rings, which is encouraged by the fact that such molecules have been shown to exhibit a wide range of biological activities.[3–10]

In this context, the antimicrobial importance of polyheterocyclic systems such as 2-quinolones is well established. The 2-quinolone moiety is among the most widely used synthetic scaffolds that researchers have used for successful design of new antimicrobial agents.[11–25] One useful strategy has been to create hybrid molecules[26] using two different pharmacophoric moieties with antimicrobial effects. 2-Quinolones could be combined with, for example, the privileged scaffolds of 1,2,3- or 1,2,4-triazoles[27–29] that have both been widely applied not only in medicinal chemistry[30–38] but also in material science.[39,40]

For instance, Ghosh and coworkers[41] reported the synthesis of novel hybrids of 1,2,4-triazolo[3,4-b][1,3,4]thiadiazines and substituted phenylquinolin-2-one moieties. The synthesized compounds exhibited moderate to good antibacterial activities against gram-positive and gram-negative bacteria. Compound I (Figure 1) showed the highest activity at the minimum inhibitory concentration (MIC) values of 1 μg/mL against *Staph-*

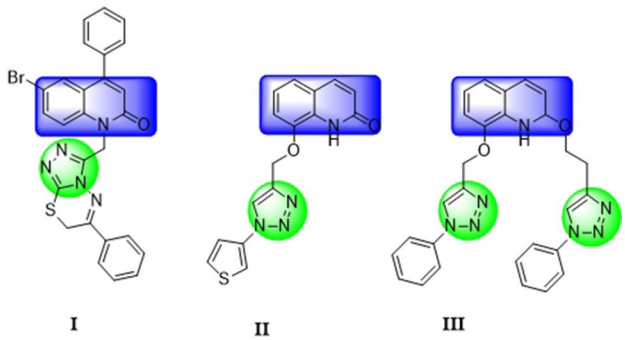

Figure 1. Some antibacterial agents based on 2-quinolone-1,2,3-triazoles.

[a] O. Moussaoui, Dr. R. Sghyar, Prof. E. M. El Hadrami, Prof. S. Chakroune
Laboratory of Applied Organic Chemistry
Sidi Mohamed Ben Abdellah University
30000 Fez (Morocco)
E-mail: oussama.moussaoui@usmba.ac.ma
[b] Dr. R. Bhadane, Dr. O. M. H. Salo-Ahen
Structural Bioinformatics Laboratory, Biochemistry
Åbo Akademi University, 20520 Turku (Finland)
E-mail: outi.salo-ahen@abo.fi
[c] Dr. R. Bhadane, Dr. O. M. H. Salo-Ahen
Pharmaceutical Sciences Laboratory, Pharmacy
Åbo Akademi University, 20520 Turku (Finland)
[d] Prof. J. Ilaš
Faculty of Pharmacy, University of Ljubljana
1000 Ljubljana (Slovenia)

Supporting information for this article is available on the WWW under https://doi.org/10.1002/cmdc.202100714

This article belongs to the Special Collection "Nordic Medicinal Chemistry"

ylococcus aureus, 2 μg/mL against *Escherichia coli* and 4 μg/mL against *Pseudomonas aeruginosa*.

Also, Gümüş and Okumuş[42] synthesized quinolone-substituted 1,2,3-triazoles. They used an efficient, alternative method for the classical copper(I)-catalyzed azide-alkyne cycloaddition reaction (CuAAC) of the mono and bis O-/N-propargylated 2-quinolone derivatives with substituted azides. The one-pot synthesis included two steps of which the first step converted the Lewis base L-proline to its catalytic salt form and the second step produced the quinolone-substituted 1,2,3-triazole derivatives resulting from the reaction of sodium azide with various aromatic and benzylic halides. The synthesized products were evaluated for their antibacterial activity against both gram-negative and gram-positive bacteria using the disk diffusion method. Compounds II and III (Figure 1) showed weak (7-mm inhibition zone) antibacterial activity against *Bacillus cereus* whereas the other compounds did not exhibit any activity against the studied bacterial strains.

The goal of the present work was to prepare novel heterocyclic hybrid antimicrobials that contain both the 2-quinolone and the 1,2,3-triazole moiety. Moreover, based on our previous work on quinoline-carboxamide derivatives of amino acids,[11] we also incorporated L-alanine, a natural amino acid into these novel compounds. Specifically, quinoline-carboxamide-L-alanine **(1 a**, **1 b)** was selected as a nucleus for the synthesis of the new compounds because it was produced with good yield and, most importantly, it showed the best antibacterial activity compared to the other studied amino acid derivatives.[11]

We have previously applied the well-known Huisgen 1,3-dipolar cycloaddition reaction[43–45] using azides as dipoles across the triple bonds of dipolarophiles for the synthesis of new hybrid triazoles.[46–48] The metal-catalyzed version of this reaction has been characterized as one of the most important tools in click chemistry[49,50] due to its "orthogonal character vs. the reactivity of most functional groups, complete regioselectivity in favor of the 1,4-disubstitued-1,2,3-triazole product, mild reaction conditions, and easy installation of the required azide and terminal alkyne moieties in the reactive partners."[51] Here, we employed the copper-catalyzed 1,3-dipolar cycloaddition reaction using propargyl-2-quinolone-L-alaninate as the dipolarophile and azides as the dipoles to synthesize novel hybrids of the two privileged scaffolds. In addition, due to the close similarity of 2-quinolones to 4-quinolones, we investigated whether these hybrid compounds could inhibit bacterial DNA gyrase to get insight into the mode of their antibacterial activity.

Results and Discussion

Synthesis of the dipolarophiles: 1-propargyl-2-oxo-1,2-dihydroquinoline-4-carboxamides 2 a/b

The reaction of the 2-quinolone derivatives with propargyl bromide under phase transfer catalysis (PTC)[52–55] conditions (liquid-solid) in dimethylformamide in the presence of potassium carbonate and tetra-n-butylammonium bromide (TBAB) led to 1-propargyl-2-quinolone (**2 a**, **2 b**) with good yields. The synthesis of the target compounds **2 a** and **2 b** was achieved by first preparing the quinolone-carboxamides **1 a** and **1 b** using the coupling reaction between 2-quinolone carboxylic acids (**a**, **b**) and L-alanine-OMe in the presence of HBTU as an activating agent and triethylamine (TEA) and chloroform ($CHCl_3$) as solvents for 12 hours at room temperature. Thereafter, an N–C bond was formed between methyl (2-oxo-1,2-dihydroquinolin-4-yl)-L-alaninate (**1 a**, **1 b**) and propargyl bromide by an N-alkylation reaction using TBAB as a catalyst and potassium carbonate (K_3CO_3) as a base in dimethylformamide (DMF) (Scheme 1).

Compounds **2 a** and **2 b** were characterized by ^1H, ^{13}C NMR spectroscopy and ESI-TOF mass-spectrometry. The ^1H NMR spectrum of 2a revealed the presence of a doublet assigned to alkyne proton CH at $\delta = 2.23$ ppm with a coupling constant $^4J = 2.4$ Hz, while two doublet of doublets signals at $\delta = 5.07$ ppm and $\delta = 4.96$ ppm illustrate the presence of the non-isochronous protons of CH_2–N with coupling constants $^4J = 2.4$ Hz and $^2J = 17.4$ Hz. In addition, the protons of the methyl group of alanine CH_3 appear in a form of a doublet at $\delta = 1.60$ ppm with a coupling constant $^3J = 7.2$ Hz. The ^{13}C NMR spectra indicate the signals of carbonyl groups of quinoline, peptide amide and the ester group at $\delta = 172.16$ ppm, $\delta = 165.66$ ppm and $\delta = 160.49$, respectively, while the quaternary carbon C–CH appears at 77.26 ppm. A signal of alkyne carbon CH resonated at $\delta =$ 72.70 ppm, whereas the signal of carbon CH_2–N appears at $\delta =$ 31.69 ppm, confirming the presence of the propargyl group. ESI-TOF mass spectrum of compound **2 a** showed $[M+Na]^+$ peak at $m/z = 365.0998$, which is in agreement with its molecular formula $C_{17}H_{16}N_2O_4$. All spectroscopic techniques used confirm the synthesis of the target compounds.

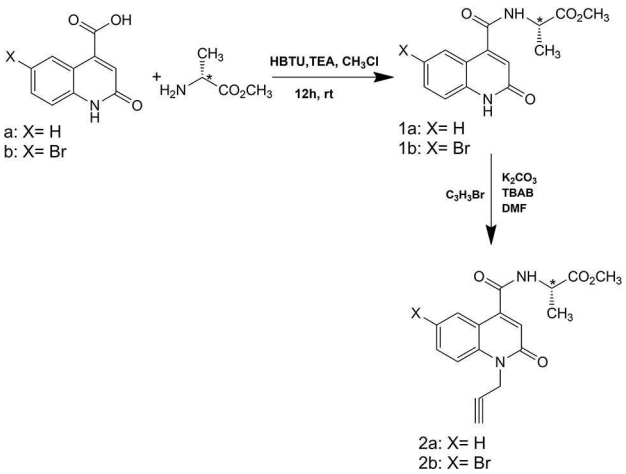

Scheme 1. Alkylation of compounds **1 a** and **1 b** with propargyl bromide.

Synthesis of hybrid quinolone-aminoester-triazoles $3a_1$–$3a_6$ and $3b_3$–$3b_4$

We then synthesized new quinolone-triazole derivatives via 1,3-dipolar cycloaddition of various azides and 1-propargyl-2-oxo-1,2-dihydroquinoline-4-carboxamides using non-catalyzed thermal activation in ethanol and a simple and inexpensive catalyst, $CuSO_4$ during 48 hours at room temperature (Scheme 2).

All newly synthesized compounds (**$3a_1$–$3a_6$** and **$3b_3$–$3b_4$**; Figure 2) were purified on liquid chromatography columns using silica gel as a stationary phase. Good yields (80%) were obtained for all other compounds except for compounds **$3a_1$** and **$3a_5$** that had a bit lower yield (75%). All compounds were characterized by ^1H, ^{13}C, DEPT, or COSY ^1H–^1H NMR and ESI-TOF mass-spectrometry.

Structural characterization of compound $3a_2$

The ^1H NMR spectrum of compound $3a_2$ (Supporting Information, p. S4) shows the presence of a doublet at $\delta = 1.57$ ppm, corresponding to the CH_3 group of the alanine with a coupling constant $^3J = 7.2$ Hz. An intense singlet signal assigned to the methoxy ester group (CH_3–O) appears at $\delta = 3.78$ ppm, while a doublet of quadruplet illustrates the presence of a proton related to the asymmetric carbon at $\delta = 4.8$ ppm with both corresponding coupling constants $^3J = 7.5$ Hz and $^3J = 7.2$ Hz. The non-isochronous protons of CH_2–$N_{quinoline}$ are manifested in a form of two doublets at $\delta = 5.29$ ppm and $\delta = 5.43$ ppm, while the singlet at $\delta = 6.77$ ppm is correlated to the ethylenic proton (=C–H) of the quinolone ring. The spectral region between $\delta =$ 7.21–7.93 ppm is assigned to aromatic protons including the singlet signal of triazole protons at $\delta = 7.48$ ppm.

According to 2D NMR spectrum (COSY ^1H–^1H) of compound **$3a_2$** (Supporting Information, p. S5), the asymmetric *CH proton of the alanine moiety presents two different coupling constants ($^3J = 7.5$ Hz and $^3J = 7.2$ Hz) confirmed by the presence of contours generally related to the neighboring N–H amide as well as the CH_3 protons of the alanine. Concerning the two non-isochronous CH_2–$N_{quinoline}$ protons, each one appears as a doublet with different chemical shifts at $\delta = 5.29$ ppm and $\delta =$ 5.43 ppm. On the other hand, the presence of two isochronous CH_2–$N_{triazole}$ protons is revealed by the singlet signal at $\delta =$ 5.37 ppm. Moreover, the proton of CH is clearly manifested by an intense and resolved singlet peak arising in the aromatic proton area at $\delta = 7.48$ ppm.

In addition, the ^{13}C NMR spectrum of compound **$3a_2$** (Supporting Information, p. S4) presents a signal related to CH_3 of the alanine group at $\delta = 18.03$ ppm, whereas the CH_2–$N_{quinoline}$ resonates at $\delta = 38.18$ ppm. The arising peak at $\delta = 48.53$ ppm is ascribed to the carbon of the methoxy group (CH_3–O), while the two deshielded signals at $\delta = 52.72$ ppm and 53.5 ppm are attributed to asymmetric carbon (*C) and –CH_2–N of the triazole, respectively. The spectral region between $\delta =$ 117–134 ppm is assigned to both aromatic and triazolic carbons, of which the latter appears at $\delta = 123.13$ ppm. The three quaternary carbons of the amide, quinoline amide and ester functional groups are confirmed by the presence of the chemical shifts at $\delta = 172.82$ ppm, $\delta = 165.87$ ppm and $\delta =$ 161.25 ppm, respectively. The chemical shifts of the proton and the tertiary carbon of the 1,2,3-triazole group are affected by the nature of the substituent on the triazole ring and thus exhibit variable values (Supporting Information, Table S1).

ESI-TOF mass spectrum of compound **$3a_2$** showed $[M + Na]^+$ peak at $m/z = 468.1642$, which is in agreement with its molecular formula $C_{25}H_{24}N_4O_4$. The structural characterization of all the other target compounds is presented in the experimental section (the NMR spectra are provided in Supporting Information, pp. S2-S17).

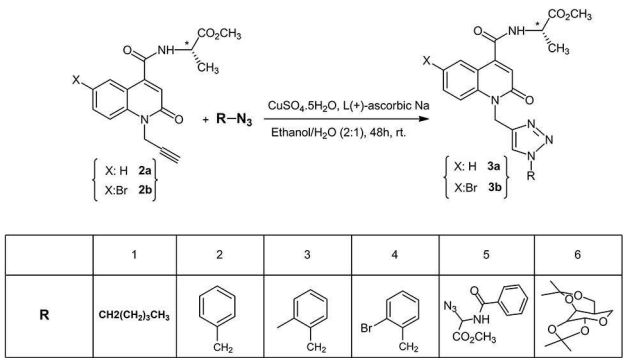

Scheme 2. Synthesis of new 1,2,3-triazole-quinolone-L-alaninate hybrids.

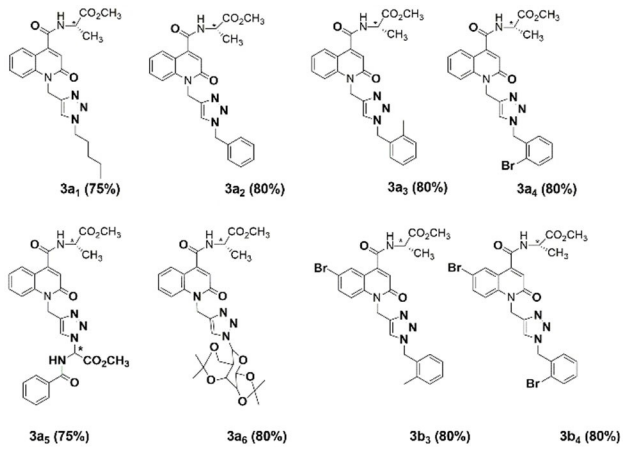

Figure 2. Structures of novel 2-quinolone-L-alaninate-1,2,3-triazoles. In all cases, the yields presented are the isolated yields after the purification.

Antibacterial activity

The newly synthesized compounds were screened for their potential antibacterial activity against *Escherichia coli* ATCC 25922, *Staphylococcus aureus* ATCC 29213, *Pseudomonas aeruginosa* ATCC 27853 and *Bacillus subtilis* ATCC 3366. Compounds were also screened for their potential antifungal activity against *Candida albicans* and *Aspergillus niger*.

The preliminary antimicrobial screening of the synthesized compounds was carried out using the disc diffusion method.[56] The diameters of the inhibition zones for the tested compounds are shown in Figure 3. Compound **3a$_4$** showed the largest diameter of the inhibition zones (d = 18 mm) against *Bacillus subtilis*. Compound **3a$_6$** formed at least a 10-mm inhibition zone against all the four bacterial strains and the two fungi, of which the largest diameters (15–16 mm) were against *Pseudomonas aeruginosa*, *Bacillus subtilis* and *Aspergillus niger*. Compounds **3a$_1$**, **3a$_4$**, **3b$_3$** and **3b$_4$** did not show any antifungal activity in this screening assay.

Thereafter the MIC values were determined with the broth microdilution method.[57] Table 1 summarizes the antibacterial and antifungal activities of the tested compounds.

Many of the compounds showed a good to moderate antibacterial and antifungal activity. Compounds **3a$_6$**, **3a$_4$** and **3b$_4$** acted as very good antibacterial agents against *B. subtilis* ATCC 3366 with MIC values of 0.039 mg/mL, 0.078 mg/mL and 0.00975 mg/mL, respectively. Likewise, compounds **3a$_3$**, **3a$_5$** and **3a$_6$** exhibited very good activity against *E. coli* ATCC 25922 with MIC values of 0.039 mg/mL, 0.0195 mg/mL and 0.00975 mg/mL, respectively. Compound **3a$_5$** showed also good activity against *S. aureus* ATCC 29213 and *P. aeruginosa* ATCC 27853 with MIC values of 0.039 mg/mL and 0.078 mg/mL, respectively. Compounds **3a$_5$** and **3a$_6$** showed altogether better antifungal activity than the rest of the compounds, although with a relatively weak effect (MIC values against *C. albicans* and *A. niger*, respectively, were as high as 5 mg/mL).

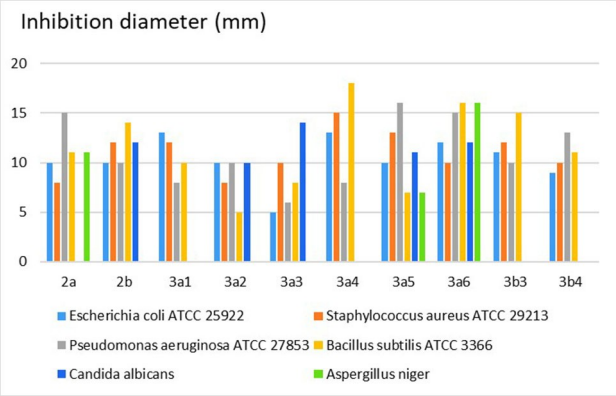

Figure 3. Results of the disc diffusion method for compounds **2a**–**2b**, **3a$_1$**–**3a$_6$** and **3b$_3$**–**3b$_4$**.

Table 1 indicates that the substituents may also affect the biological activity of the synthesized compounds **3a$_1$**–**3a$_6$** and **3b$_1$**–**3b$_6$**. Comparison of the antibacterial activities of the tested compounds suggests that the substituents R/X=C_7H_6Br/Br convey potent antibacterial activity against *B. subtilis*. The substituents R/X = galactose/H cause a higher antibacterial activity against *E. coli* than what the other compounds have, perhaps due to the presence of the glucide group that may have a role in the bactericidal mechanism. Also, the groups R/X = glycinate/H convey potent antibacterial activity against *S. aureus* and P. aeruginosa, possibly due to the asymmetric group. Moreover, the substituents R/X = galactose/H and glycinate/H have positional interference, as can be observed from the antifungal activity results of the corresponding compounds against *A. niger* and *C. albicans*, respectively.

DNA gyrase inhibition

Since 2-quinolones resemble 4-quinolones such as the fluoroquinolone ciprofloxacin and aminocoumarins such as novobiocin, we wanted to investigate whether our hybrid compounds could inhibit the same target as ciprofloxacin and novobiocin, i.e., DNA gyrase, the bacterial type II topoisomerase.[58,59] We first carried out molecular docking studies of the synthesized hybrid compounds at the crystal structures of *E. coli* and *S. aureus* DNA gyrase. We hypothesized that these compounds might preferably bind into the fluoroquinolone site in the gyrase A subunit (GyrA) or the coumarin binding site in the gyrase B subunit (GyrB). However, we also investigated their binding at the so-called novel bacterial topoisomerase inhibitor (NBTI) binding site formed between the two GyrA subunits.[60] The docking results clearly suggest that our novel compounds would not have a good binding affinity or interactions at any of these binding sites, compared to the reference inhibitors obtained from their respective DNA gyrase crystal complexes (for the detailed analysis, please see Supporting Information, pp. S18–S23, Tables S2, S3 and Figures S1–S5).

We then determined the inhibitory activities of our compounds against *E. coli* DNA gyrase in supercoiling/relaxation assays. The assay results confirmed our prediction: no compound showed DNA gyrase inhibition at 100 μM concentration.

Table 1. Antibacterial and antifungal activities as minimum inhibitory concentration (MIC, mg/mL) of compounds 2a, 2b, 3a$_1$–3a$_6$ and 3b$_3$–3b$_4$.

Compound	Escherichia coli ATCC 25922	Staphylococcus aureus ATCC 29213	Pseudomonas aeruginosa ATCC 27853	Bacillus subtilis ATCC 3366	Candida albicans	Aspergillus niger.
2a	0.62	2.5	0.62	5	NA	10
2b	0.62	2.5	2.5	2.5	10	NA
3a$_1$	0.078	1.25	2.5	0.31	NA	NA
3a$_2$	0.31	2.5	2.5	2.5	10	NA
3a$_3$	0.039	1.25	1.25	2.5	10	NA
3a$_4$	2.5	0.31	2.5	0.078	NA	NA
3a$_5$	0.0195	0.039	0.078	0.31	5	10
3a$_6$	0.00975	0.078	0.62	0.039	10	5
3b$_3$	0.62	2.5	0.62	0.31	NA	NA
3b$_4$	0.31	2.5	1.25	0.00975	NA	NA

In silico characterization of the novel hybrid compounds

We further characterized the novel quinolone-triazole derivatives using different computational tools. We employed quantum mechanics (QM) to calculate the compounds' pK_a values and possible tautomers in water. The pK_a prediction was performed for the C=O group of the 2-quinolone moiety, the N–N=N and C–N=N groups of the triazole ring, and NH of the amide groups of the synthesized compounds (Table 2). The pK_a values are very low for the 'basic' groups (carbonyl oxygen/triazole nitrogens) (Table 2), which means that they either do not get protonated at all at pH range 1–14 (those with negative pK_a values) or it protonates only (partially) at very low pH (the nitrogen atoms with positive pK_a values). The C–N=N nitrogen of **3a**$_1$ has the highest pK_a, suggesting that of all the compounds it is the most protonated at pH 1–2. Furthermore, the amide NH is so weakly acidic (i.e., has high pK_a values) that it will not be able to donate its proton in the physiological pH range. Consequently, if taken orally, absorption of these novel compounds (in the unprotonated form) could start slowly already in the stomach and would then continue in the small intestine where the compounds are completely unprotonated and, thus, can penetrate the epithelial cell membrane well. The tautomer prediction suggests that none of the novel compounds has tautomers in water (Supporting Information, Table S5).

In addition, during the QM geometry optimization, the highest occupied (HOMO) and the lowest unoccupied (LUMO) molecular orbitals were calculated to evaluate the stability of the compounds. As electrons are constantly shuttling between the molecular orbitals, the smaller the gap between these orbitals is, the more easily they can jump between the different states. These molecular orbitals are concentrated on the pi-electron-rich quinolone ring system, indicating a good conjugation network in this region (Supporting Information, Figure S6). This conveys the compounds the ability to absorb light at longer wavelengths, which provides additional stability to the molecules upon exposure to UV radiation. Thus, the smaller the gap between HOMO and LUMO energies is the more stable the compound is. In general, the molecular orbital energies are relatively similar between the compounds. Compound **3a**$_5$ had the smallest HOMO-LUMO energy gap, while compound **3a**$_1$ had the largest energy gap (Supporting Information, Table S5).

We also predicted a range of pharmacokinetic and toxicity properties (ADMET properties; absorption, distribution, metabolism, excretion, and toxicity) of the novel compounds. Overall, the ADMET predictions suggest no apparent toxicity to host cells. The predicted values of various selected properties are shown in Table 3. None of the compounds is predicted to be CNS (central nervous system) active although compound **3a**$_3$ is predicted to greatly penetrate the blood-brain barrier (BBB) as suggested by the highest value for the model cell (MDCK, Madin-Darby Canine Kidney) permeability. On the other hand, compound **3a**$_5$ is predicted to have the poorest BBB penetration. All of these compounds are predicted to inhibit hERG (human ether-à-go-go-related gene) potassium channels of the heart, which could render them as cardiotoxic. All compounds are predicted to be absorbed from the intestine, compounds **3a**$_4$ and **3b**$_3$ having the best predicted apparent Caco-2 cell permeability. Compound **3a**$_5$, however, has a significantly lower

Table 2. Predicted pK_a values of the synthesized compounds.

Compound	pK_a C=O[a] (basic)	N–N=N (basic)	C–N=N (basic)	NH[b] (acidic)
3a$_{1s}$	−2.2	−1.05	2.31	15.62
3a$_2$	−3.41	−2.76	0.94	15.38
3a$_3$	−2.58	−1.78	1.16	14.84
3a$_4$	–[c]	−1.79	1.04	15.44
3a$_5$	−2.28	−2.59	1.05	19.94/12.78[d]
3a$_6$	−2.3	−3.62	0.97	16.01
3b$_3$	−2.91	−1.59	1.88	14.81
3b$_4$	−2.91	−1.62	1.23	15.11

Colour scheme: green for higher and yellow for lower values. Notes: [a] C=O in the 2-quinolone ring; [b] amide NH of the L-alaninate moiety; [c] not possible to determine; [d] NH of the benzamide moiety.

Table 3. Various ADMET properties of the synthesized compounds predicted by QikProp.

Compound	CNS activity[a]	hERG blockage (log IC_{50})[b]	Apparent Caco-2 permeability (nm/s)[c]	Apparent MDCK permeability (nm/s)[d]	Skin permeability (log K_p)[e]	Aqueous solubility (log S)[f]	Number of reactive functional groups[g]	Number of likely metabolic reactions[h]
3a$_1$	−2	−6.085	294	132	−3.026	−5.348	1	2
3a$_2$	−2	−7.098	257	114	−2.642	−5.831	1	3
3a$_3$	−2	−6.232	206	90	−3.048	−5.269	1	4
3a$_4$	−2	−6.619	340	320	−2.588	−5.966	1	3
3a$_5$	−2	−7.705	50	19	−3.831	−6.631	2	3
3a$_6$	−2	−6.234	269	120	−3.513	−6.193	4	2
3b$_3$	−2	−6.484	344	812	−2.735	−6.992	1	4
3b$_4$	−2	−6.691	179	205	−3.32	−6.708	1	3

[a] Predicted central nervous system activity; scale: –2 (inactive) to +2 (active); [b] hERG: Gene encoding protein of the alpha subunit of a potassium ion channel; hERG blockers are cardiotoxic (concern below −5); [c] Caco-2: human colon carcinoma cell line used to model intestinal absorption (<25 poor; >500 great); [d] MDCK: Madin-Darby Canine Kidney cell line used to model the blood-brain barrier (<25 poor; >500 great); [e] Range for 95% of known drugs −8.0–(−1.0); [f] Aqueous solubility (S) in mol/dm^3 is the concentration of the solute in a saturated solution that is in equilibrium with the crystalline solid. Log S range for 95% of known drugs: −6.5 to 0.5; [g] The presence of reactive functional groups can lead to false positives in High-Throughput Screening assays and to decomposition, reactivity, or toxicity problems *in vivo* (95% of known drugs have 0–2 reactive groups); [h] For 95% of known drugs the number of metabolic reactions varies between 1 and 8.

predicted Caco-2 permeability than the other compounds in this series.

All compounds are predicted to have a relatively good skin permeability. Their aqueous solubility is predicted to be low and especially compounds **3b$_3$** and **3b$_4$** with the halogen substituted quinolone ring show the lowest predicted water solubility. As a reactive group, all compounds have an unhindered ester (**3a$_5$** has two of them) and **3a$_6$** has also 3 acetal-type of groups. Furthermore, one of the likely metabolic pathways for the compounds could be e.g., the oxidation of the benzylic carbon.

Conclusions

In this work, we present the synthesis of new quinolone-aminoester-triazole hybrid molecules **3a$_1$**–**3a$_6$** and **3b$_3$**–**3b$_4$** with good yields. The triple bond of two types of quinolone-carboxamides was reacted with different types of substituted azides (including sugar, amino ester, aromatic and alkyl groups) using click chemistry and Cu(I) as a catalyst. All compounds were obtained with excellent purity and have been characterized by ^{1}H and ^{13}C, DEPT, or COSY ^{1}H–^{1}H NMR and ESI-TOF mass spectrometry.

The potential antibacterial activity of the compounds was tested against *Escherichia coli* ATCC 25922, *Staphylococcus aureus* ATCC 29213, *Pseudomonas aeruginosa* ATCC 27853 and *Bacillus subtilis* ATCC 3366, and their antifungal activity was tested against *Candida albicans* and *Aspergillus niger*. Many of the compounds showed moderate to good activities against one or more of the bacterial strains whereas only some of the compounds showed weak to moderate antifungal activity. The most potent and broad-spectrum compounds were **3a$_5$** and **3a$_6$**, exhibiting antimicrobial activity against all these organisms.

The presence of 1,2-dihydroquinoline moiety led us to explore the bacterial DNA gyrase as the primary target for these compounds. Unfortunately, none of these compounds inhibited DNA gyrase, suggesting that they have a different mechanism of bacterial inhibition. Finally, computational prediction of the pharmacokinetic and toxicity properties of the compounds suggests that they have potential to be optimized and used as new pharmacophores for development of antibacterial and antifungal therapeutic agents.

Experimental Section

Chemistry

Materials and instruments. The following reagents used for the synthesis were purchased from Sigma-Aldrich: triethylamine 99.5%, hexafluorophosphate benzotriazole tetramethyl uronium (HBTU) 98% and L-alanine 99%, tetra-n-butylammonium bromide (BTBA) 90%, propargyl bromide 80% in toluene, potassium carbonate (K_2CO_3) 99%, copper sulfate pentahydrate ($CuSO_4.5H_2O$) 99% and L(+)-ascorbic acid sodium salt and analytical solvents such as ethanol 99.5%, anhydrous dimethylformamide 99.8%, ethyl acetate (HPLC-grade) and hexane (HPLC-grade). Column liquid chromatography was performed on 60 Merck silica gel (230–400 mesh ASTM). Thin layer chromatography (TLC) was performed on Merck aluminum plates coated with 60 F254 Merck silica gel (thickness 0.2 mm). The synthesized components were revealed by an ultra-violet lamp set at 254 nm and their melting points were determined by Electrothermal IA 9000 Series digital fusiometer using capillary tubes. NMR spectra and ESI-TOF mass spectroscopy were recorded at the Department of Chemistry, University of Helsinki, Finland. NMR spectra were performed on Bruker Ascend 400 MHz-Avance III HD NMR spectrometer (Bruker Corporation, Billerica, MA, USA). ^{1}H NMR spectra were recorded at 400 MHz, and ^{13}C NMR spectra at 100 MHz using DMSO-d_6 or $CDCl_3$ as the solvent. The chemical shift (δ) of different peaks was expressed in ppm and the coupling constants (^{n}J) in Hz. For describing the multiplicity of signals, the following abbreviations have been used: singlet (s), doublet (d), doublet of doublet (dd), doublet of doublet of doublet (ddd), multiplet (m), triplet (t) and quadruplet (q). The high-resolution mass spectra were measured by the micro TOF-MS instrument (Bruker Daltonics GmbH, Bremen, Germany) in positive electrospray ionization mode. During the pre-measurement, the instrument was calibrated with the 5 mM sodium formate solution.

Procedure for the preparation of 2a and 2b

A mixture of methyl (2-oxo-1.2-dihydroquinolin-4-yl)-L-alaninate **1** (1.5 mmol) and of potassium carbonate (K_2CO_3) (3 mmol) is dissolved in 25 ml of dimethylformamide (DMF). The solution is magnetically stirred for 5 minutes, then 0.01 equivalent of tetra-n-butylammonium bromide (TBAB) and 3 mmol of propargyl bromide are added. The mixture is magnetically stirred for 6 hours. After filtration of the salts, DMF is evaporated under reduced pressure. The residue obtained is dissolved in dichloromethane and washed with water. The organic phase is dried on Na_2SO_4 and then concentrated under vacuum. The residue obtained is purified by chromatography on a silica gel column.

General procedure for the preparation of 3a$_1$–3a$_6$ and 3b$_3$–3b$_4$

1 mmol of compound **2** is added to 2 mmol of azide in a mixture of ethanol/water (2/1: v/v) at room temperature. 0.1 mmol of copper sulphate pentahydrate ($CuSO_4.5H_2O$) and 1 mmol of sodium ascorbate are added to the flask. The reaction is stirred for 48 hours. After evaporation of ethanol, the mixture is extracted with dichloromethane and dried with Na_2SO_4, followed by evaporation of the dichloromethane. The product is purified by chromatography on a silica gel column with a hexane/ethyl (2/1: v/v) acetate eluent.

Methyl (S)-2-[2-oxo-1-(prop-2-yn-1-yl)-1,2-dihydroquinoline-4-carbox amido]propanoate (2a): Yield: 80%; white solid; mp = 166–168 °C; R_f = 0.4 (hexane/ethyl acetate 1/1: v/v). ***^{1}H NMR*** (400 MHz, **$CDCl_3$**): 8.00 (dd, 1H, ^{3}J = 8.1 Hz, ^{4}J = 1.2 Hz, H_{ar}), 7.66 (td, 1H, ^{3}J = 7.2 Hz, ^{4}J = 1.5 Hz, H_{ar}), 7.52 (dd, 1H, ^{3}J = 8.1 Hz, ^{4}J = 1.5 Hz, H_{ar}), 7.33 (td, 1H, $^3J_{H-H}$ = 7.2 Hz, $^4J_{H-H}$ = 1.2 Hz, H_{ar}), 7.88 (d, 1H, $^3J_{H-H}$ = 7.2 Hz, NH), 6.82 (s, 1H, $CH_{ethylenic}$), 5.07(dd, 1H, $^2J_{H-H}$ = 17.4 Hz, $^4J_{H-H}$ = 2.4 Hz, CH_2–$N_{quinoline}$), 4.96 (dd, 1H, $^2J_{H-H}$ = 17.4 Hz, $^4J_{H-H}$ = 2.4 Hz, CH_2–$N_{quinoline}$), 4.84 (qd, 1H, $^3J_{H-H}$ = 7.2 Hz, $^3J_{H-H}$ = 7.2 Hz, *CH–N), 3.84 (s, 3H, CH_3–O), 2.23 (t, 1H, $^4J_{H-H}$ = 2.4 Hz, CH), 1.60 (d, 3H, $^3J_{H-H}$ = 7.2 Hz, CH_3). ***^{13}C NMR*** (100 MHz, **$CDCl_3$**): 172.16 (C=O_{ester}), 165.66 (C=O_{amide}) (C=$O_{amide\ quinoline}$), 160.49, 145.35–138.94 (C_{4a} and C_{8a}), 131.59 (Ct_5), 127.36 (Ct_7), 123.16 (=$Ct_{ethylenic}$), 119.38 (Ct_6), 117.73 ($Cq_{ethylenic}$),115.03 (Ct_8), 77.26(Cq_{alkyne}), 72.70 (CH_{Alkyne}), 52.75 (*CH–N), 48.55 (CH_3–O), 31.69 (CH_2–$N_{quinoline}$), 18.6 (CH_3). ***Mass spectrometry (ESI-TOF-MS)***: *m/z* calculated for [C17H16 N2O4 + Na]$^+$35.1002, found 335.0998, *m/z* calculated for [(C17H16 N2O4)2 + Na] + 647.2112, found 647.2112.

Methyl (S)-6-bromo-2-[2-oxo-1-(prop-2-yn-1-yl)-1,2-dihydroquinoline-4-carboxamido]propanoate (2b): Yield: 80%; white solid; mp = 178–180 °C; R_f = 0.4 (hexane/ethyl acetate 1/1: v/v). ***^{1}H NMR*** (400 MHz, $CDCl_3$): 8.1 (d, 1H, ^2J = 2.1 Hz, H_{ar}), 7.76 (td, 1H, ^3J = 7.2 Hz, ^4J = 2.1 Hz, H_{ar}), 7.62 (d, 1H, ^3J = 7.2 Hz, H_{ar}), 7.14 (d, 1H, $^3J_{H-H}$ = 7.2 Hz, NH), 6.9 (s, 1H, $CH_{ethylenic}$), 5.07(d, 1H, $^2J_{H-H}$ = 17.4 Hz, $^4J_{H-H}$ = 2.4 Hz, CH_2–$N_{quinoline}$), 4.96 (d, 1H, $^2J_{H-H}$ = 17.4 Hz, $^4J_{H-H}$ = 2.4 Hz, CH_2–$N_{quinoline}$), 4.84 (qd, 1H, $^3J_{H-H}$ = 7.2 Hz, $^3J_{H-H}$ = 7.2 Hz, *CH–N), 3.84 (s, 3H, CH_3–O), 2.23 (t, 1H, $^4J_{H-H}$ = 2.4 Hz, CH), 1.60 (d, 3H, $^3J_{H-H}$ = 7.2 Hz, CH_3). ***^{13}C NMR*** (100 MHz, $CDCl_3$): 174.2 ($C{=}O_{ester}$), 167.66 ($C{=}O_{amide}$), 161.49 ($C{=}O_{amide}$), 145.85–138.74 (C_{4a} and C_{8a}), 131.59 (Ct_5), 127.36 (Ct_7), 123.16 (=$Ct_{ethylenic}$), 119.38 (Ct_6), 117.73 ($Cq_{ethylenic}$), 117.65 (Cq_{ar}), 115.03 (Ct_8), 77.70 (Cq_{alkyne})72.70 (CH_{alkyne}), 52.75 (*CH–N), 48.55 (CH_3–O), 31.69(CH_2–$N_{quinoline}$), 18.6 (CH_3). ***Mass spectrometry (ESI-TOF-MS)***: *m/z* calculated for $[C_{17}H_{15}BrN_2O_4+Na]^+$ 413.0125, found 413.0138, *m/z* calculated for $[(C_{17}H_{15}N_2O_4)_2+Na]^+$ 805.0358, found 805.0312.

Methyl (S)-2-{2-oxo-1-[(1-pentyl-1H-1,2,3-triazol-4-yl)methyl]-1,2-dihy droquinoline-4-carboxamido}propanoate ($3a_1$): Yield: 75%; white solid; mp = 180–12 °C; R_f = 0.2 (hexane/ethyl acetate 1/2: v/v). ***^{1}H NMR*** (400 MHz, $CDCl_3$): 7.94 (dt, 1H, ^3J = 8.1 Hz, ^4J = 1.8 Hz, H_{ar}), 7.64 (m, 2H, H_{ar}), 7.59 (s, 1H, $H_{triazole}$), 7.28 (m, 1H, H_{ar}), 6.85 (s, 1H, $CH_{ethylenic}$), 6.76 (d, 1H, $^3J_{H-H}$ = 7.5 Hz, NH), 5.58 (d, 1H, $^2J_{H-H}$ = 20.5 Hz, CH_2–$N_{quinoline}$), 5.57 (d, 1H, $^2J_{H-H}$ = 20.5 Hz, CH_2–$N_{quinoline}$), 4.85 (qd, 1H, $^3J_{H-H}$ = 7.5 Hz, $^3J_{H-H}$ = 7.2 Hz, *CH–N), 4.85 (t, 2H, $^3J_{H-H}$ = 7.4 Hz, CH_2–$N_{triazole}$), 3.84 (s, 3H, CH_3–O), 1.86 (tt, 2H, $^3J_{H-H}$ = 8.27 Hz, $^3J_{H-H}$ = 7.4 Hz, CH_2–$N_{quinoline}$), 1.86 (m, 2H, CH_2), 1.59 (d, 3H, $^3J_{H-H}$ = 7.2 Hz, CH_3), 0.86 (t, 3H, $^3J_{H-H}$ = 6.2 Hz, CH_3). ***^{13}C NMR*** (100 MHz, $CDCl_3$): 172.82 ($C{=}O_{ester}$), 165.78 ($C{=}O_{amide\ quinoline}$), 161.32 ($C{=}O_{amide}$), 145.39–138.52 (C_{4a},C_{8a} and $Cq_{triazole}$), 131.91 (Ct_5), 127.00 (Ct_7), 123.16 (=$Ct_{ethylenic}$), 122.80 ($Ct_{triazole}$), 119.28 (Ct_6), 117.51 ($Cq_{ethylenic}$),115.69 (Ct_8), 52.75 (*CH–N), 50.50 (CH_2–N), 48.55 (CH_3–O), 38.43 (CH_2-$_{triazole}$), 29.71 (CH_2), 28.56 (CH_2), 22.03 (CH_2), 18.6 (CH_3), 13.80 (CH_3). **Mass spectrometry (ESI-TOF-MS)**: *m/z* calculated for $[C_{22}H_{27}N_5O_4+Na]^+$ 48.1955, found 448,1950, *m/z* calculated for $[(C_{22}H_{27}BrN_5O_4)_2+Na]^+$ 873.4024, found 873.3999.

Methyl (S)-2-{2-oxo-1-[(1-benzyl-1H-1,2,3-triazol-4-yl)methyl]-1,2-dih ydroquinoline-4-carboxamido}propanoate ($3a_2$): Yield: 80%; white solid; mp = 168–170 °C; R_f = 0.15 (hexane/ethyl acetate 1/2: v/v). ***^{1}H NMR*** (400 MHz, $CDCl_3$): 7.92 (dt, 1H, ^3J = 8.1 Hz, ^4J = 1.5 Hz, H_{ar}), 7.86(d, 1H, ^3J = 8.62 Hz, H_{ar}), 7.60 (td, ^{1}H, ^3J = 8.7, ^3J = 7.2, ^4J = 1.5 Hz, H_{ar}), 7.48 (s, 1H, $H_{triazole}$), 7.36–7.21 (m, 6H, H_{ar}), 7.11 (d, 1H, $^3J_{H-H}$ = 7.5 Hz, NH), 6.76 (s, 1H, $CH_{ethylenic}$), 5.57–5.28 (m, 4H, CH_2–N), 4.85 (qd, 1H, $^3J_{H-H}$ = 7.5 Hz, $^3J_{H-H}$ = 7.2 Hz, *CH–N), 3.78 (s, 3H, CH_3–O), 2.19 (s, 3H, CH_3-Ar), 1.56 (d, 3H, $^3J_{H-H}$ = 7.2 Hz, CH_3). ***^{13}C NMR*** (100 MHz, $CDCl_3$): 172.82 ($C{=}O_{ester}$), 165.87 ($C{=}O_{amide}$), 161.25 ($C{=}O_{amide}$), 145.49–138.52 (C_{4a},$C_{8a\ and}$ $Cq_{triazole}$), 134 (Ct_{benz}), 131.84 (Ct_5), 129.12 (Ct_{benz}), 128.81 (Ct_{benz}), 128.20 (Ct_{benz}), 127.07 (Ct_7), 123.25 (=$Ct_{ethylenic}$), 123.13 ($Ct_{triazole}$), 119.12 (Ct_6), 117.57 ($Cq_{ethylenic}$),115.69 (Ct_8), 53.5 (CH_2–$N_{triazole}$), 52.72 (*CH–N), 48.53 (CH_3–O), 38.18 (CH_2–N), 18.03 (CH_3). ***Mass spectrometry (ESI-TOF-MS)***: *m/z* calculated for $[C_{24}H_{23}N_5O_4+Na]^+$468.1642, found 468.1642, *m/z* calculated for $[(C_{24}H_{23}N_5O_4)_2+Na]^+$913.3392, found 913.3392.

Methyl (S)-2-{2-oxo-1-[(1-(2-methylbenzyl)-1H-1,2,3-triazol-4-yl)meth yl]-1,2-dihydroquinoline-4-carboxamido}propanoate ($3a_3$): Yield: 80%; white solid; mp = 215–217 °C; R_f = 0.15 (hexane/ethyl acetate 1/2: v/v). ***^{1}H NMR*** (400 MHz, $CDCl_3$): 8.08 (m, 1H, H_{ar}), 7.85 (d, ^{1}H, ^3J = 9 Hz, H_{ar}), 7.71 (td, 1H, ^3J = 9 Hz, ^2J = 2.2 Hz, H_{ar}), 7.64 (s, 1H, $H_{triazole}$), 7.43–7.38 (m, 2H, H_{ar}), 6.83 (s, 1H, $CH_{ethylenic}$), 6.74 (d, 1H, $^3J_{H-H}$ = 7.4 Hz, NH), 5.57–5.50 (m, 4H, CH_2–N), 4.82 (qd, 1H, $^3J_{H-H}$ = 7.5 Hz, $^3J_{H-H}$ = 7.2 Hz, *CH–N), 3.85 (s, 3H, CH_3–O), 1.67 (s, 3H, CH_3-Ar), 1.59 (d, 3H, $^3J_{H-H}$ = 7.2 Hz, CH_3). ***^{13}C NMR DEPT 135°*** (100 MHz, $CDCl_3$): 134.72 (Ct_{benz}), 129.49 (Ct_5), 128.86 (Ct_7), 124.39 (=$Ct_{ethylenic}$), 123.76 ($Ct_{triazole}$), 120.33 (Ct_{benz}), 117.12 (Ct_6), 112.63 (Ct_8), 53.28 (CH_2–$N_{triazole}$), 52.40 (*CH–N), 46.6 (CH_3–O), 38.46 (CH_2–N), 18.23 (CH_3), 18.24 (CH_3). ***Mass spectrometry (ESI-TOF-MS)***: *m/z* calculated for $[C_{25}H_{25}N_5O_4+Na]^+$482.1799, found 482.1799, *m/z* calculated for $[(C_{25}H_{25}N_5O_4)_2+Na]^+$941.3705, found 941.3705.

Methyl (S)-2-{2-oxo-1-[(1-(2-bromobenzyl)-1H-1,2,3-triazol-4-yl)meth yl]-1,2-dihydroquinoline-4-carboxamido}propanoate ($3a_4$): Yield: 80%; white solid; mp = 166–168 °C; R_f = 0.1 (hexane/ethyl acetate 1/2: v/v). ***^{1}H NMR*** (400 MHz, $CDCl_3$): 7.94 (m, 2H, H_{ar}), 7.61–7.19 (m, 8H, $H_{triazole}$ and H_{ar}), 7.12 (d, 1H, $^3J_{H-H}$ = 7.5 Hz, NH), 6.82 (s, 1H, $CH_{ethylenic}$), 5.61 (s, 2H, CH_2-Ar), 5.51 (d, 1H, J = 18 Hz, CH_2–$N_{quinoline}$), 5.34 (d, 1H, J = 18 Hz, CH_2–$N_{quinoline}$), 4.85 (qd, 1H, $^3J_{H-H}$ = 7.5 Hz, $^3J_{H-H}$ = 7.2 Hz, *CH–N), 3.84 (s, 3H, CH_3–O), 1.6 (d, 3H, $^3J_{H-H}$ = 7.2 Hz, CH_3). ***^{13}C NMR*** (100 MHz, $CDCl_3$): 172.79 ($C{=}O_{ester}$), 165.9 ($C{=}O_{amide}$), 161.24 ($C{=}O_{amide}$), 145.49–139.18 ((C_{4a},C_{8a} and $Cq_{triazole}$), 133.26 (Cq_{ar}), 134 (Ct_{benz}), 131.87 (Ct_5), 130.46 (Ct_{benz}), 130.40 Ct_{benz}), 128.21(Ct_{benz}), 127.03 (Ct_7), 123.56 (=$Ct_{ethylenic}$), 123.10 ($Ct_{triazole}$), 119.27 (Ct_6), 117.52 ($Cq_{ethylenic}$),115.69 (Ct_8), 53.91 (CH_2–$N_{triazole}$), 52.78 (*CH–N), 48.53 (CH_3–O), 38.33 (CH_2–$N_{quinoline}$), 18.6 (CH_3). ***Mass spectrometry (ESI-TOF-MS)***: *m/z* calculated for $[C_{25}H_{22}BrN_5O_4+Na]^+$546.0747, found 546.0747, *m/z* calculated for $[(C_{25}H_{25}N_5O_4)_2+Na]^+$1069.1603, found 1069.1603.

Methyl (S)-2-{2-oxo-1-[(1-(1-benzamido-2-methoxy-2-oxoethyl)-1H-1,2,3-triazol-4-yl)methyl]-1,2-dihydroquinoline-4-carboxamido}propanoate ($3a_5$): Yield: 75%; white solid, mp = 123–125 °C; R_f = 0.15 (hexane/ethyl acetate 1/2: v/v). ***^{1}H NMR*** (400 MHz, $CDCl_3$): 8.05 (s, 1H, NH), 7.92 (t, 1H, $^3J_{H-H}$ = 9.3 Hz, H_{ar}), 7.92 (td, 1H, $^3J_{H-H}$ = 7.3 Hz, $^4J_{H-H}$ = 1.8 Hz, H_{ar}), 7.59 (m, 2H, H_{ar}), 7.45 (m, 2H, H_{ar} and $H_{triazole}$), 7.26 (d, 1H, $^3J_{H-H}$ = 7.5 Hz, H_{ar}), 6.98 (d, 1H, $^3J_{H-H}$ = 7.9 Hz, NH), 6.82 (d, 1H, $^3J_{H-H}$ = 2.7 Hz, *CH–$N_{triazole}$), 6.71 (s, 1H, $CH_{ethylenic}$), 5.59 (s, 2H, CH_2–$N_{triazole}$), 4.85 (qd, 1H, $^3J_{H-H}$ = 7.7 Hz, $^3J_{H-H}$ = 6.5 Hz, *CH–N), 3.86 (s, 3H, CH_3–O), 3.84 (d, 3H, $^3J_{H-H}$ = 1.5 Hz, CH_3–O), 1.6 (d, 3H, $^3J_{H-H}$ = 7.2 Hz, CH_3). ***^{13}C NMR*** (100 MHz, $CDCl_3$): 172.75 ($C{=}O_{ester}$), 166.78 ($C{=}O_{amide}$), 166.43($C{=}O_{amide}$), 165.80 ($C{=}O_{amide}$), 165.40 ($C{=}O_{ester}$), 161.24 ($C{=}O_{ester}$), 145.49–139.55 (C_{4a},C_{8a} and $Cq_{triazole}$), 138.77 (Ct_{benz}), 134.24 (Ct_{benz}), 132.82 (Cq_{ar}), 131.87 (Ct_5)„ 128.21 (Ct_{benz}), 127.03 (Ct_7), 123.56 (=$Ct_{ethylenic}$), 121.10 ($Ct_{triazole}$), 119.35 (Ct_6), 117.56 ($Cq_{ethylenic}$),115.59 (Ct_8), 53.91 (CH_2–$N_{triazole}$), 52.78 (*CH–N), 48.53 (CH_3–O), 38.33 (CH_2–$N_{quinoline}$), 18.6 (CH_3). ***Mass spectrometry (ESI-TOF-MS)***: *m/z* calculated for $[C_{27}H_{26}N_6O_7+Na]^+$ 569.1755, found 569.1764, *m/z* calculated for $[(C_{27}H_{26}N_6O_7)_2+Na]^+$ 15.3618, found 1115.3618.

Methyl (S)-2-{2-oxo-1-[(1–(2-oxo-1–2,2,8,8-tetramethylhexahydro-[1,3]dioxolo[4′, 5′:5,6]pyrano[4,3-d][1,3]dioxin-5-yl)-1H-1,2,3-triazol-4-yl)methyl]-1,2-dihydroquinoline-4-carboxamido}propanoate ($3a_6$): Yield: 80%; white solid; mp = 128–130 °C; R_f = 0.15 (hexane/ethyl acetate 1/2: v/v). ***^{1}H NMR*** (400 MHz, $CDCl_3$): 7.92 (dd, 1H, $^3J_{H-H}$ = 8.1 Hz, ^4J = 1.5 Hz, H_{ar}), 7.75 (d, 1H, $^3J_{H-H}$ = 8.6 Hz, H_{ar}), 7.61–7.53 (m, 2H, H_{ar} et $H_{triazole}$), 7.45 (d, H, $^3J_{H-H}$ = 7.4 Hz, NH), 7.31–7.20 (m, 2H, H_{ar}), 6.75 (s, 1H, $H_{ethylenic}$), 5.42 (d, 1H, $^3J_{H-H}$ = 5.7 Hz, CH), 5.42 (d, 1H, $^3J_{H-H}$ = 16 Hz, CH_2–$N_{quinoline}$), 5.09 (d, 1H, $^3J_{H-H}$ = 16 Hz, CH_2–$N_{quinoline}$), 4.85 (qd, 1H, $^3J_{H-H}$ = 7.4 Hz, $^3J_{H-H}$ = 7.2 Hz, *CH–N), 4.58 (dd, 1H, $^3J_{H-H}$ = 7.7 Hz,^{4}J = 2.5 Hz, CH), 4.46 (dd, 1H, $^3J_{H-H}$ = 14.2 Hz, ^4J = 4.1 Hz, CH), 4.32 (m, 1H, CH), 4.27 (dd, 1H, $^3J_{H-H}$ = 5.1 Hz, ^4J = 2.5 Hz, CH), 3.8 (s, 3H, CH_3–O), 1.6 (d, 3H, $^3J_{H-H}$ = 7.2 Hz, CH_3), 1.58 (s, 3H, CH_3), 1.43 (s, 3H, CH_3), 1.30 (s, 6H, CH_3), 1.26 (s, 6H, CH_3). ***^{13}C NMR DEPT 135°*** (100 MHz, $CDCl_3$): 131.74 (Ct_5), 127.12 (Ct_7), 124.57 (=$Ct_{ethylenic}$), 123.09($Ct_{triazole}$), 119.02 (Ct_6), 115.58 (Ct_8), 96.12 ($Cq_{galactose\ anomeric\ carbon}$), 66.95 ($CH_2$–O), 52.66 ($CH_2$–$N_{triazole}$), 50.39 (*CH–N), 48.54 (CH_3–O), 38.01 (CH_2–N), 25.91 (CH_3), 25.79 (CH_3), 24.84 (CH_3), 24.37 (CH_3), 17.84 (CH_3). ***Mass spectrometry (ESI-TOF-MS)***: *m/z* calculated for $[C_{29}H_{34}N_5O_9+Na]^+$620. 2337, found 620. 2337, *m/z* calculated for $[(C_{29}H_{34}N_5O_9)_2+Na]^+$1217.4780, found 1217.4780.

Methyl (S)-6-bromo-2-{2-oxo-1-[(1-(2-methylbenzyl)-1H-1,2,3-triazol-4-yl)methyl]-1,2-dihydroquinoline-4-carboxamido}propanoate (3b$_3$): Yield: 80%; white solid; mp = 245–247 °C; R_f = 0.15 (hexane/ethyl acetate 1/2: v/v). ***^{1}H NMR*** (400 MHz, $CDCl_3$): 8.08 (d, $^4J_{H-H}$ = 2.3 Hz, 1H, H_{ar}), 7.88 (d, 1H, $^3J_{H-H}$ = 9 Hz, H_{ar}), 7.70 (dd, 1H, $^3J_{H-H}$ = 9.1 Hz, ^4J = 2.3 Hz, H_{ar}), 7.43 (s, 1H, $H_{triazole}$), 7.31–7.26 (m, 1H, H_{ar}), 7.22–7.13 (m, 3H, H_{ar}), 6.82 (s, 1H, $CH_{ethylenic}$), 6.66 (d, 1H, $^3J_{H-H}$ = 7.5 Hz, NH), 5.59 (m, 4H, CH_2), 4.82 (qd, 1H, $^3J_{H-H}$ = 7.2 Hz, $^3J_{H-H}$ = 7.5 Hz, *CH–N), 3.85 (s, 3H, CH_3–O), 2.27 (s, 1H, CH_3-Ar), 1.58 (d, 3H, $^3J_{H-H}$ = 7.2 Hz, CH_3). ***^{13}C NMR DEPT 135°*** (100 MHz, $CDCl_3$): 134.64 (Ct_5), 131.39 (Ct_{benz}), 129.66 (Ct_7), 129.36 (Ct_{benz}), 129.30 (Ct_{benz}), 126.74 (Ct_{benz}), 123.13 ($Ct_{triazole}$), 120.43 (Ct_6), 117.42 (=$Ct_{ethylenic}$), 52.87 (*CH–N), 52.42 (CH_2–$N_{triazole}$), 48.59 (CH_3–O), 38.26 (CH_2–$N_{quinoline}$), 19.03 (CH_3-Ar), 18.27 (CH_3). ***Mass spectrometry (ESI-TOF-MS)***: *m/z* calculated for $[C_{25}H_{21}Br_2N_4O_4 + Na]^+$560.0789, found 560.0918, *m/z* calculated for $[(C_{25}H_{21}Br_2N_4O_4)_2 + Na]^+$1097,1621, found 1097.

Methyl (S)-6-bromo-2-{2-oxo-1-[(1-(2-bromobenzyl)-1H-1,2,3-triazol-4-yl)methyl]-1,2-dihydroquinoline-4-carboxamido}propanoate (3b$_4$): Yield: 80%; white solid; mp = 230–232 °C; R_f = 0.15 (hexane/ethyl acetate 1/2: v/v). ***^{1}H NMR*** (400 MHz, $CDCl_3$): 8.10 (s, 1H, H_{ar}), 7.96 (m, 1H, H_{ar}), 7.72 (s, 1H, $H_{triazole}$), 7.62 (d, 1H, $^3J_{H-H}$ = 7.8 Hz, H_{ar}), 7.31 (m, 1H, H_{ar}), 7.22 (t, 1H, $^3J_{H-H}$ = 7.6 Hz), 6.89 (s, 1H, $CH_{ethylenic}$), 6.69 (d, 1H, $^3J_{H-H}$ = 6.9 Hz, NH), 5.61–5.12 (m, 4H, CH_2), 4.84 (qd, 1H, $^3J_{H-H}$ = 7.2 Hz, $^3J_{H-H}$ = 6.9 Hz, *CH–N), 3.85 (s, 3H, CH_3–O), 1.58 (d, 3H, $^3J_{H-H}$ = 7.2 Hz, CH_3). ***^{13}C NMR DEPT 135°*** (100 MHz, $CDCl_3$): 134.81 (Ct_5), 133.26 (Ct_{benz}), 130.65 (Ct_{benz}), 130.63 (Ct_{benz}), 129.39 (Ct_7), 128.21 (Ct_{benz}), 123.13 ($Ct_{triazole}$), 122.28 (Ct_6), 118.96 (=$Ct_{ethylenic}$), 52.89 (*CH–N), 52.72 (CH_2–$N_{triazole}$), 46.6 (CH_3–O), 38.46 (CH_2–$N_{quinoline}$), 18.31 (CH_3). ***Mass spectrometry (ESI-TOF-MS)***: *m/z* calculated for $[C_{25}H_{21}Br_2N_4O_4 + Na]^+$623.9787, found 623.9869, *m/z* calculated for $[(C_{25}H_{21}Br_2N_4O_4)_2 + Na]^+$1226.9780, found 1226.9805.

Antimicrobial activity evaluation

The Agar Disc Diffusion Method (ADD) was employed for the determination of antibacterial activities of the tested products as described previously. The test samples were first dissolved in dimethyl sulfoxide (1%) (DMSO), which did not affect the microbial growth. Briefly, the test was performed on sterile petri plates containing agar medium. 30 ml of the sterilized medium was poured into sterile petri plates. After solidification, 100 µl of fresh cultures of bacterial species (one microorganism per petri plate) was added onto the plates. Sterile filter paper discs (6 mm in diameter) were impregnated with 6 µl of 10 mg/mL test samples. All plates were sealed with sterile laboratory films to avoid eventual evaporation of the test samples, and then incubated at 37 °C for 24 h.[56] The diameter of the inhibition zone was measured in millimeters and an average of three independent determinations was recorded.

The MICs of **2a**, **2b**, **3a$_1$**–**3a$_6$** and **3b$_3$**–**3b$_4$** were determined by the broth microdilution method.[57,61] A 96-well polypropylene microtiter plate was filled with 50 µL of Mueller-Hinton broth (MHB). Then, 50 µL of each sample at a final concentration of 10 mg/mL was added into the first well. Serial $^1/_2$ dilutions were realized by pipetting 50 µL from the first well and transferred to the next one. This operation was repeated until the 12th well and the last 50 µL mixture was discarded. Finally, a volume of 50 µL of bacterial suspension was added into each well at a final concentration of approximately 10^6 CFU/mL. The 96-well plate was then covered and was incubated at 37 °C for 24 h, whereas plates containing fungal organisms were incubated at 28 °C for 48 h. After that, 5 µL of resazurin was pipetted into all the wells and incubated once more at 37 °C for 2 h. The MIC is presented as the lowest concentration that showed a negative bacterial growth, detected as a non-change in resazurin color. A positive bacterial growth was observed as a reduction of the blue dye resazurin to pink resorufin.[57,61] The MIC determination was performed in triplicate for each organism and the experiment was repeated where necessary.

Computational studies

Ligand and protein preparation: The 2D structures of the synthesized hybrid compounds were prepared with ChemDraw version 19.1 and imported into Maestro (Schrödinger Release 2020–4: Maestro, Schrödinger, LLC, New York, NY, 2020). The 2D structures were converted to 3D using Maestro's LigPrep tool: possible tautomeric states for each ligand were generated at pH 7.0 ± 2.0 with Epik[62] and maximum of two stereoisomers were generated per ligand; the OPLS3e force field[63] was applied to generate optimized low-energy 3D conformers of the ligands. We used only the S enantiomers of the amino acid (L-alanine) moiety and the SS stereoisomer of 3a$_5$ for the computational studies.

The crystal structures of two *S. aureus* and one *E. coli* DNA gyrase-inhibitor complexes (PDB ID: 5BS3[64] – a complex with a novel bacterial topoisomerase inhibitor [NBTI], resolution 2.65 Å; 5CDQ[65] – a complex with moxifloxacin, a fluoroquinolone, res. 2.95 Å; 4DUH[66] – a complex with a 4,5′-bithiazole inhibitor [4′-methyl-N(2)-phenyl-[4,5′-bithiazole]-2,2′-diamine], res. 1.5 Å, respectively) were retrieved from the Protein Data Bank (PDB).[67] The target structures were processed with the Protein Preparation Wizard[68] of Maestro. The missing hydrogen atoms were added and the hydrogen bond network was optimized with PROPKA at pH 7.0. All water molecules beyond 3 Å from non-protein atoms were removed and a restrained minimization was carried out using the OPLS3e force field with the convergence criteria of 0.3 Å RMSD for all heavy atoms.

Mapping water interaction sites at the quinolone and NBTI binding pockets: Since the crystal resolution is somewhat low for the *S. aureus* DNA gyrase-inhibitor complexes (PDB IDs: 5BS3 and 5CDQ) only a few or no crystal water molecules are detected at the NBTI or fluoroquinolone binding sites in the DNA gyrase subunit A (GyrA). The coumarin binding site in the DNA gyrase subunit B (GyrB) of the *E. coli* structure (PDB ID: 4DUH), however, contains co-crystallized water molecules. To investigate whether water plays an important role in mediating the inhibitor binding interactions, we calculated favorable water interaction fields at the NBTI and fluoroquinolone binding sites using the program GRID (version 22d)[69–71] of Molecular Discovery Ltd. The probing area for detecting possible hydration layers was restricted to cover the area around the particular co-crystallized ligand. The number of planes per Ångström and resolution was set to 0.25 Å. The energy minima below −7 kcal/mol in the Grid map were detected with the program MINIM, whereafter the program FILMAP was used to populate the energy minima with water molecules. The subsequent docking studies at the three inhibitor binding sites (NBTI, fluoroquinolone, coumarin) were performed both with and without the GRID-calculated/crystal water molecules for the reference compounds (Supporting Information, p. S19, Figure S2, Table S2) and with the water molecules for the novel synthesized compounds. For the binding free energy evaluation, these favorable water molecules were included for all compounds.

Molecular docking: Docking was performed with the extra precision (XP) mode of Glide[72–74] (Schrödinger Release 2020-4: Glide, Schrödinger, LLC, New York, NY, 2020) at the three ligand binding sites defined by the co-crystallized inhibitors in the selected DNA gyrase structures. The outer box size of the docking grid was set to 30 Å × 30 Å × 30 Å (the diameter midpoint of the docked ligands was set to remain in an inner box with dimensions of 10 Å × 10 Å × 10 Å). Flexible ligand sampling was used and for each ligand 10

poses were taken for post-docking minimization and one pose per ligand was generated. The Epik state penalties were added to the final docking score. The docking protocol was validated by docking the co-crystallized ligands back into their crystal binding sites (Supporting Information, p. S18, Figure S1).

Binding free energy prediction: The Prime[75,76]/MM-GBSA tool of Maestro Schrödinger Release 2020–4: Prime, Schrödinger, LLC, New York, NY, 2020) was used to calculate the binding free energies for the docked poses of the synthesized compounds. The binding free energy ΔG_{bind} is estimated according to [Eq. (1)]:

$$\Delta G_{bind=}\Delta E_{MM} + \Delta G_{solv} + \Delta G_{SA} \quad (1)$$

where ΔE_{MM} is the difference in energy between the complex structure and the sum of the energies of the ligand and unliganded receptor (in the OPLS3e molecular mechanics force field), ΔG_{solv} is the difference in the generalized Born surface area (GBSA) solvation energy of the complex and the sum of the solvation energies for the ligand and unliganded receptor (calculated with the VSGB2.1 solvation model[77]), and ΔG_{SA} is the difference in the surface area energy for the complex and the sum of the surface area energies for the ligand and uncomplexed receptor.

Quantum mechanical calculations: All the 3D structures of the synthesized compounds that were initially generated and optimized in the OPLS3e force field were subjected to *ab initio* quantum mechanical (QM) geometry optimization using Jaguar (Schrödinger Release 2020-4: Jaguar, Schrödinger, LLC, New York, NY, 2020).[78] The 6–31G** basis set was used with the B3LYP–D3[79] density functional theory (DFT) with automatic self-consistent field (SCF) spin treatment using medium grid density with nonrelativistic Hamiltonian. Geometry optimization in the gas phase was carried out for 100 steps with default convergence criteria. The highest and lowest occupied molecular orbitals (HOMO and LUMO, respectively) were calculated. The pK_a values of the compounds were predicted using the Jaguar pK_a prediction tool.[80,81] The selection of atoms for pK_a prediction was made automatically in water. Maximum of 48 iterations with DIIS convergence scheme were performed. The tautomer prediction was done using the Jaguar QM conformer and tautomer prediction tool. The top five tautomers were allowed to be generated in water without charge adjustment using the default workflow.

ADME and toxicity prediction: Schrödinger's QikProp tool (Schrödinger Release 2020–4: QikProp, Schrödinger, LLC, New York, NY, 2020) was used to predict pharmacokinetic properties of the synthesized compounds.

Determination of inhibitory activities on *E. coli* DNA gyrase

Inhibitory activities against *E. coli* DNA gyrase were determined in supercoiling or relaxation assays from Inspiralis on streptavidin-coated 96-well microtiter plates from Thermo scientific Pierce. First, the plates were rehydrated with buffer (20 mM Tris-HCl with pH 7.6, 0.01% w/v BSA, 0.05% v/v Tween 20, 137 mM NaCl) and the biotinylated oligonucleotide was then immobilized. After washing off the unbound oligonucleotide, the enzyme test was performed. The reaction volume of 30 μL in buffer (35 mM Tris × HCl with pH 7.5, 4 mM MgCl2, 24 mM KCl, 2 mM DTT, 1.8 mM spermidine, 1 mM ATP, 6.5% w/v glycerol, 0.1 mg/mL) contained 1.5 U of DNA gyrase from *E. coli*, 0.75 μg of relaxed pNO1 plasmid, and 3 μL solution of the inhibitor in 10% DMSO and 0.008% Tween 20. Reaction solutions were incubated at 37 °C for 30 min. After that, the TF buffer (50 mM NaOAc with pH 5.0, 50 mM NaCl and 50 mM MgCl2) was added to terminate the enzymatic reaction. After additional incubation for 30 min at rt, during which biotin-oligonucleotide-plasmid triplex was formed, the unbound plasmid was washed off using TF buffer and SybrGOLD in T10 buffer (10 mM Tris HCl with pH 8.0 and 1 mM EDTA) was added. The fluorescence was measured with a microplate reader (BioTek Synergy H4, excitation: 485 nm, emission: 535 nm). Initial screening was done at 100 or 10 μM concentration of inhibitors against *E. coli* DNA gyrase. Novobiocin (IC_{50} = 0.168 μM [lit. 0.08 μM])[82] was used as the positive control.

Acknowledgements

We acknowledge the great support from the Department of Chemistry, University of Helsinki, Finland. Specifically, we would like to thank Mr. Hassan Haddad, Ms. Karina Moslova and all researchers of the Department of Chemistry at the University of Helsinki for providing the necessary tools to conduct this research. Financial support from Tor, Joe and Pentti Borg's Memorial Foundation to R.B. and Slovenian Research Agency for J.I. (Grant No. P1-0208) is gratefully acknowledged. The Sigrid Jusélius Foundation, Biocenter Finland Bioinformatics and Drug Discovery and Chemical Biology networks, CSC IT Center for Science, and Prof. Mark Johnson and Dr. Jukka Lehtonen are acknowledged for the excellent computational infrastructure at the Åbo Akademi University. This work contributes also to the activities within the strategic research profiling area Solutions for Health at Åbo Akademi University (Academy of Finland, #336355).

Conflict of Interest

The authors declare no conflict of interest.

Data Availability Statement

The data that support the findings of this study are available in the supplementary material of this article.

Keywords: 2-quinolone derivatives · 1,2,3-triazole · 1,3 dipolar cycloaddition · antibacterial activity · DNA gyrase · molecular modeling

[1] J. O'Neill, Tackling Drug-Resistant Infections Globally: Final Report and Recommendations, Review On Antimicrobial Resistance, **2016**.
[2] S. Correia, P. Poeta, M. Hébraud, J. L. Capelo, G. Igrejas, *J. Med. Microbiol.* **2017**, *66*, 551–559.
[3] P. Villa, N. Arumugam, A. I. Almansour, R. Suresh Kumar, S. M. Mahalingam, K. Maruoka, S. Thangamani, *Bioorg. Med. Chem. Lett.* **2019**, *29*, 729–733.
[4] B. Alcaide, P. Almendros, C. Aragoncillo, *Curr. Opin. Drug Discovery Dev.* **2010**, *13*, 685–697.
[5] R. da Silva Mesquita, A. Kyrylchuk, I. Grafova, D. Kliukovskyi, A. Bezdudnyy, A. Rozhenko, W. P. Tadei, M. Leskelä, A. Grafov, *PLoS One* **2020**, *15*, e0227811.
[6] O. A. El-Sayed, B. A. Al-Bassam, M. E. Hussein, *Arch. Pharm.* **2002**, *335*, 403–410.
[7] A. Mahamoud, J. Chevalier, A. Davin-Regli, J. Barbe, J.-M. Pages, *Curr. Drug Targets* **2006**, *7*, 843–847.
[8] J. C. S. Bergh, T. H. Tötterman, B. C. Termander, K. A.-M. P. Strandgarden, P. O. G. Gunnarsson, B. I. Nilsson, *Cancer Invest.* **1997**, *15*, 204–211.

[9] A. Trivedi, D. Dodiya, J. Surani, S. Jarsania, H. Mathukiya, N. Ravat, V. Shah, *Arch. Pharm.* **2008**, *341*, 435–439.
[10] T. A. Rano, E. Sieber-McMaster, P. D. Pelton, M. Yang, K. T. Demarest, G.-H. Kuo, *Bioorg. Med. Chem. Lett.* **2009**, *19*, 2456–2460.
[11] O. Moussaoui, E. M. El Hadrami, G. Benjalloune Touimi, B. Bennani, A. Ben Tama, S. Chakroune, A. Boukir, *Mediterr. J. Chem.* **2019**, *9*, 326–336.
[12] O. Moussaoui, R. Bhadane, R. Sghyar, E. M. El Hadrami, S. El Amrani, A. Ben Tama, Y. Kandri Rodi, S. Chakroune, O. M. H. Salo-Ahen, *Sci. Pharm.* **2020**, *88*, 57.
[13] K. C. Sekgota, S. Majumder, M. Isaacs, D. Mnkandhla, H. C. Hoppe, S. D. Khanye, F. H. Kriel, J. Coates, P. T. Kaye, *Bioorg. Chem.* **2017**, *75*, 310–316.
[14] P. A. Sakharov, N. V. Rostovskii, A. F. Khlebnikov, T. L. Panikorovskii, M. S. Novikov, *Org. Lett.* **2019**, *21*, 3615–3619.
[15] A. A. Aly, E. A. Ishak, A. M. Shwaky, A. H. Mohamed, *Monatsh. Chem.* **2020**, *151*, 223–229.
[16] M. S. Katagi, J. Fernandes, S. Mamledesai, D. Satyanarayana, P. Dabadi, G. Bolakatti, *J. Pharm. Res.* **2015**, *14*, 51–56.
[17] W. Xue, X. Li, G. Ma, H. Zhang, Y. Chen, J. Kirchmair, J. Xia, S. Wu, *Eur. J. Med. Chem.* **2020**, *188*, 112022.
[18] H. Govender, C. Mocktar, H. M. Kumalo, N. A. Koorbanally, *Phosphorus Sulfur Silicon Relat. Elem.* **2019**, *194*, 1074–1081.
[19] O. V. Elenich, R. Z. Lytvyn, O. V. Blinder, O. V. Skripskaya, O. S. Lyavinets, K. E. Pitkovych, M. D. Obushak, P. I. Yagodinets, *Pharm. Chem. J.* **2019**, *52*, 969–974.
[20] M. D. Ferretti, A. T. Neto, A. F. Morel, T. S. Kaufman, E. L. Larghi, *Eur. J. Med. Chem.* **2014**, *81*, 253–266.
[21] Q. Deng, Q.-G. Ji, Z.-Q. Ge, X.-F. liu, D. Yang, L.-J. Yuan, *Med. Chem. Res.* **2014**, *23*, 5224–5236.
[22] N. J. Parmar, B. R. Pansuriya, B. D. Parmar, H. A. Barad, *Med. Chem. Res.* **2014**, *23*, 42–56.
[23] R. V. Patel, P. Kumari, D. P. Rajani, K. H. Chikhalia, *J. Fluorine Chem.* **2011**, *132*, 617–627.
[24] I. Stepanenko, S. Yamashkin, Y. Kostina, A. Batarsheva, M. Mironov, *Res. Results Pharmacol.* **2018**, *4*, 27–36.
[25] P. K. Patel, R. V. Patel, D. H. Mahajan, P. A. Parikh, G. N. Mehta, C. Pannecouque, E. De Clercq, K. H. Chikhalia, *J. Heterocycl. Chem.* **2014**, *51*, 1641–1658.
[26] Shaveta, S. Mishra, P. Singh, *Eur. J. Med. Chem.* **2016**, *124*, 500–536.
[27] L. S. M. Forezi, C. G. S. Lima, A. A. P. Amaral, P. G. Ferreira, M. C. B. V. Souza, A. C. Cunha, F. C. da Silva, V. F. Ferreira, *Chem. Rec.* **2021**, *21*, 2782–2807.
[28] R. Gondru, S. Kanugala, S. Raj, C. Ganesh Kumar, M. Pasupuleti, J. Banothu, R. Bavantula, *Bioorg. Med. Chem. Lett.* **2021**, *33*, 127746.
[29] C. Tratrat, *Curr. Top. Med. Chem.* **2020**, *20*, 2235–2258.
[30] K. T. Petrova, T. M. Potewar, P. Correia-da-Silva, M. T. Barros, R. C. Calhelha, A. Ćiric, M. Soković, I. C. F. R. Ferreira, *Carbohydr. Res.* **2015**, *417*, 66–71.
[31] G. Turan-Zitouni, Z. A. Kaplancıklı, M. T. Yıldız, P. Chevallet, D. Kaya, *Eur. J. Med. Chem.* **2005**, *40*, 607–613.
[32] R. Lakkakula, A. Roy, K. Mukkanti, G. Sridhar, *Russ. J. Gen. Chem.* **2019**, *89*, 831–835.
[33] M. K. Mohammed, Z. Al-Shuhaib, A. A. A. Al-Shawi, *Mediterr. J. Chem.* **2019**, *9*, 305–310.
[34] J. Gour, S. Gatadi, V. Pooladanda, S. M. Ghouse, S. Malasala, Y. V. Madhavi, C. Godugu, S. Nanduri, *Bioorg. Chem.* **2019**, *93*, 103306.
[35] R.-Z. Huang, G.-B. Liang, M.-S. Li, Y.-L. Fang, S.-F. Zhao, M.-M. Zhou, Z.-X. Liao, J. Sun, H.-S. Wang, *MedChemComm* **2019**, *10*, 584–597.
[36] M. Whiting, J. Muldoon, Y.-C. Lin, S. M. Silverman, W. Lindstrom, A. J. Olson, H. C. Kolb, M. G. Finn, K. B. Sharpless, J. H. Elder, V. V. Fokin, *Angew. Chem. Int. Ed.* **2006**, *45*, 1435–1439; *Angew. Chem.* **2006**, *118*, 1463–1467.
[37] E. Cichero, L. Buffa, P. Fossa, *J. Mol. Model.* **2011**, *17*, 1537–1550.
[38] G. R. Labadie, A. de la Iglesia, H. R. Morbidoni, *Mol. Diversity* **2011**, *15*, 1017–1024.
[39] J. Huo, H. Hu, M. Zhang, X. Hu, M. Chen, D. Chen, J. Liu, G. Xiao, Y. Wang, Z. Wen, *RSC Adv.* **2017**, *7*, 2281–2287.
[40] A. Diaz-Ortiz, P. Prieto, J. R. Carrillo, R. Martin, I. Torres, *Curr. Org. Chem.* **2015**, *19*, 568–584.
[41] S. Ghosh, A. Verma, A. Mukerjee, M. K. Mandal, *Arab. J. Chem.* **2019**, *12*, 3046–3053.
[42] A. Gümüs, V. Okumuş, *Turk. J. Chem.* **2018**, *42*, 1344–1357.
[43] R. Huisgen, *Angew. Chem.* **1963**, *75*, 604–637; *Angew. Chem. Int. Ed.* **1963**, *2*, 565–598.
[44] R. Huisgen, *J. Org. Chem.* **1976**, *41*, 403–419.
[45] K. V. Gothelf, K. A. Jørgensen, *Chem. Rev.* **1998**, *98*, 863–910.
[46] I. Fichtali, M. Chraibi, F. E. Aroussi, A. Bentama, E. M. E. Hadrami, K. F. Benbrahim, S.-E. Stiriba, *Der Pharma Chemica* **2016**, *8*, 236–242.
[47] L. Bahsis, H. Ben El Ayouchia, H. Anane, C. Ramirez de Arellano, A. Bentama, E. El Hadrami, M. Julve, L. Domingo, S.-E. Stiriba, *Catalysts* **2019**, *9*, 687.
[48] N. Agouram, E. M. E. Hadrami, A. B. Tama, M. Julve, H. Anane, S.-E. Stiriba, *Der Pharma Chemica* **2016**, *8*, 499–506.
[49] V. V. Rostovtsev, L. G. Green, V. V. Fokin, K. B. Sharpless, *Angew. Chem. Int. Ed. Engl.* **2002**, *41*, 2596–2599.
[50] C. W. Tornøe, C. Christensen, M. Meldal, *J. Org. Chem.* **2002**, *67*, 3057–3064.
[51] A. Mandoli, *Molecules* **2016**, *21*, 1174.
[52] M. Makosza, *Pure Appl. Chem.* **1975**, *43*, 439–462.
[53] M. Mąkosza, M. Fedoryński, in: *Encyclopedia of Catalysis* (Ed.: I. Horváth), John Wiley & Sons, Inc., Hoboken, NJ, USA, **2010**, p. eoc170.pub2.
[54] A. Keita, F. Lazrak, E. M. Essassi, I. C. Alaoui, Y. K. Rodi, J. Bellan, M. Pierrot, *Phosphorus Sulfur Silicon Relat. Elem.* **2003**, *178*, 1541–1548.
[55] O. Moussaoui, S. Byadi, M. Eddine Hachim, R. Sghyar, L. Bahsis, K. Moslova, A. Aboulmouhajir, Y. K. Rodi, Č. Podlipnik, E. M. E. Hadrami, S. Chakroune, *J. Mol. Struct.* **2021**, *1241*, 130652.
[56] M. R. S. Zaidan, A. Noor Rain, A. R. Badrul, A. Adlin, A. Norazah, I. Zakiah, *Trop. Biomed.* **2005**, *22*, 165–170.
[57] W. Ouedrhiri, S. Bouhdid, M. Balouiri, A. E. O. Lalami, S. Moja, F. O. Chahdi, H. Greche, *J. Chem. Pharm. Res.* **2015**, *7*, 78–84.
[58] L. Costenaro, J. G. Grossmann, C. Ebel, A. Maxwell, *Structure* **2007**, *15*, 329–339.
[59] F. Collin, S. Karkare, A. Maxwell, *Appl. Microbiol. Biotechnol.* **2011**, *92*, 479–497.
[60] B. D. Bax, P. F. Chan, D. S. Eggleston, A. Fosberry, D. R. Gentry, F. Gorrec, I. Giordano, M. M. Hann, A. Hennessy, M. Hibbs, J. Huang, E. Jones, J. Jones, K. K. Brown, C. J. Lewis, E. W. May, M. R. Saunders, O. Singh, C. E. Spitzfaden, C. Shen, A. Shillings, A. J. Theobald, A. Wohlkonig, N. D. Pearson, M. N. Gwynn, *Nature* **2010**, *466*, 935–940.
[61] D. F. Basri, C. K. Luoi, A. M. Azmi, J. Latip, *Pharmaceuticals* **2012**, *5*, 1032–1043.
[62] J. C. Shelley, A. Cholleti, L. L. Frye, J. R. Greenwood, M. R. Timlin, M. Uchimaya, *J. Comput.-Aided Mol. Des.* **2007**, *21*, 681–691.
[63] K. Roos, C. Wu, W. Damm, M. Reboul, J. M. Stevenson, C. Lu, M. K. Dahlgren, S. Mondal, W. Chen, L. Wang, R. Abel, R. A. Friesner, E. D. Harder, *J. Chem. Theory Comput.* **2019**, *15*, 1863–1874.
[64] S. B. Singh, D. E. Kaelin, J. Wu, L. Miesel, C. M. Tan, T. Black, R. Nargund, P. T. Meinke, D. B. Olsen, A. Lagrutta, J. Lu, S. Patel, K. W. Rickert, R. F. Smith, S. Soisson, E. Sherer, L. A. Joyce, C. Wei, X. Peng, X. Wang, H. Fukuda, R. Kishii, M. Takei, H. Takano, M. Shibasaki, M. Yajima, A. Nishimura, T. Shibata, Y. Fukuda, *Bioorg. Med. Chem. Lett.* **2015**, *25*, 1831–1835.
[65] P. F. Chan, V. Srikannathasan, J. Huang, H. Cui, A. P. Fosberry, M. Gu, M. M. Hann, M. Hibbs, P. Homes, K. Ingraham, J. Pizzollo, C. Shen, A. J. Shillings, C. E. Spitzfaden, R. Tanner, A. J. Theobald, R. A. Stavenger, B. D. Bax, M. N. Gwynn, *Nat. Commun.* **2015**, *6*, 10048.
[66] M. Brvar, A. Perdih, M. Renko, G. Anderluh, D. Turk, T. Solmajer, *J. Med. Chem.* **2012**, *55*, 6413–6426.
[67] H. M. Berman, J. Westbrook, Z. Feng, G. Gilliland, T. N. Bhat, H. Weissig, I. N. Shindyalov, P. E. Bourne, *Nucleic Acids Res.* **2000**, *28*, 235–242.
[68] G. Madhavi Sastry, M. Adzhigirey, T. Day, R. Annabhimoju, W. Sherman, *J. Comput.-Aided Mol. Des.* **2013**, *27*, 221–234.
[69] P. J. Goodford, *J. Med. Chem.* **1985**, *28*, 849–857.
[70] R. C. Wade, P. J. Goodford, *J. Med. Chem.* **1993**, *36*, 148–156.
[71] R. C. Wade, K. J. Clark, P. J. Goodford, *J. Med. Chem.* **1993**, *36*, 140–147.
[72] R. A. Friesner, J. L. Banks, R. B. Murphy, T. A. Halgren, J. J. Klicic, D. T. Mainz, M. P. Repasky, E. H. Knoll, M. Shelley, J. K. Perry, *J. Med. Chem.* **2004**, *47*, 1739–1749.
[73] T. A. Halgren, R. B. Murphy, R. A. Friesner, H. S. Beard, L. L. Frye, W. T. Pollard, J. L. Banks, *J. Med. Chem.* **2004**, *47*, 1750–1759.
[74] R. A. Friesner, R. B. Murphy, M. P. Repasky, L. L. Frye, J. R. Greenwood, T. A. Halgren, P. C. Sanschagrin, D. T. Mainz, *J. Med. Chem.* **2006**, *49*, 6177–6196.
[75] M. P. Jacobson, R. A. Friesner, Z. Xiang, B. Honig, *J. Mol. Biol.* **2002**, *320*, 597–608.
[76] M. P. Jacobson, D. L. Pincus, C. S. Rapp, T. J. F. Day, B. Honig, D. E. Shaw, R. A. Friesner, *Proteins* **2004**, *55*, 351–367.
[77] J. Li, R. Abel, K. Zhu, Y. Cao, S. Zhao, R. A. Friesner, *Proteins Struct. Funct. Bioinf.* **2011**, *79*, 2794–2812.

[78] A. D. Bochevarov, E. Harder, T. F. Hughes, J. R. Greenwood, D. A. Braden, D. M. Philipp, D. Rinaldo, M. D. Halls, J. Zhang, R. A. Friesner, *Int. J. Quantum Chem.* **2013**, *113*, 2110–2142.
[79] S. Grimme, J. Antony, S. Ehrlich, H. Krieg, *J. Chem. Phys.* **2010**, *132*, 154104.
[80] D. M. Philipp, M. A. Watson, H. S. Yu, T. B. Steinbrecher, A. D. Bochevarov, *Int. J. Quantum Chem.* **2018**, *118*, e25561.
[81] A. D. Bochevarov, M. A. Watson, J. R. Greenwood, D. M. Philipp, *J. Chem. Theory Comput.* **2016**, *12*, 6001–6019.
[82] S. Alt, L. A. Mitchenall, A. Maxwell, L. Heide, *J. Antimicrob. Chemother.* **2011**, *66*, 2061–2069.

Manuscript received: November 13, 2021
Revised manuscript received: December 16, 2021
Accepted manuscript online: January 2, 2022
Version of record online: January 27, 2022